Pulsed Magnetoplasmadynamic Detonation Propulsion

IEPC-2007-199

Presented at the 30th International Electric Propulsion Conference, Florence, Italy
September 17-20, 2007

Kyoichi Kuriki*, Junichiro Aoyagi† and Haruki Takegahara‡
Tokyo Metropolitan University, Tokyo, 191-0065, Japan.

Abstract: One-dimensional magnetoplasmadynamic detonation was formulated and solved for jump conditions corresponding to the Chapman-Jouguet point. A thruster design guideline was suggested referring to high enthalpy plasma produced behind strong detonation. The Alfvén's critical velocity ionization was found closely related to the Chapman-Jouguet detonation condition.

I. Introduction

"STRIKE while the iron is hot" is a design principle of electric propulsion. It is requisite to minimize plasma loss and heat transfer to thruster wall by either accelerating the plasma instantly after production or confining prior to acceleration. The former design option, an objective of present study, has been applied to the development of pulsed plasma thruster (PPT), while the latter to the ion engine. The PPT has been employed in flight systems[1] taking advantage of ablative solid propellant, although further efforts have been desired to make the system more attractive. The one of the efforts is to make specific impulse controllable by varying the average feed rates of gas propellant and electrical energy. Such performance can be attained by repetitively pulsed magnetoplasmadynamic (MPD) thruster with steady gas supply. The other effort is to find a design guideline for the improvement of propulsion efficiency. In the present study is proposed a detonation model for gas fed pulsed MPD thruster to suggest a design guideline.

So far the pulsed plasma acceleration has been understood by the models of the slug flow, snowplow and gasdynamic shock wave[2]. In these models the front of arc discharge is regarded as a magnetic piston, which eventually ejects the one shot mass or the entrained gas initially filling a discharge chamber. Present model is similar to the gasdynamic shock model which assumes a shock wave driven by the magnetic piston. In this study, instead of the shock wave, introduced is a detonation wave which ionizes and magnetizes the entrained gas in a discharge current sheet. In order to find MPD jump conditions the conventional analyses of combustion detonation[3] are generalized by the use of electrical input energy and MPD thermodynamic relations[4]. Once the plasma state behind the MPD detonation wave is obtained, one can reflect the results in the thruster design as to enhance propulsive performance. Although complex discharge patterns were observed experimentally[5], simple one-dimensional model is expected to provide a basic approach.

II. Pulsed Magnetoplasmadynamic Propulsion

Basic arrangements of the pulsed MPD propulsion are illustrated in Fig. 1. Energy storage, a pulse forming network (PFN) delivers a current pulse of duration τ to parallel plate electrodes. The electrodes are closed with an

* Visiting Professor, Dept. Aerospace Engineering, kuriki@astak3.tmit.ac.jp
† Assistant professor, Dept. Aerospace Engineering, j-aoyagi@astak3.tmit.ac.jp
‡ Professor, Dept. Aerospace Engineering, hal@astak3.tmit.ac.jp

insulator wall at an end $x = 0$ and assumed sufficiently long until scale criteria will be discussed. The inter-electrode region is filled with stationary gas before firing. When switch SW is turned on, an avalanche break down occurs on the insulator surface and an MPD detonation wave is driven by the magnetic piston along the electrodes. The setup other than the energy storage in Fig. 1 is regarded as a reaction chamber for combustible gas propellant. After the combustion is ignited on the end wall, a combustion detonation wave moves along the parallel plates and eventually fills the chamber with motionless burnt gas. Similarity between the two processes above suggests the applicability of conventional combustion detonation analysis to the pulsed MPD detonation by taking the energy emerging in the unit mass of propellant as a common parameter.

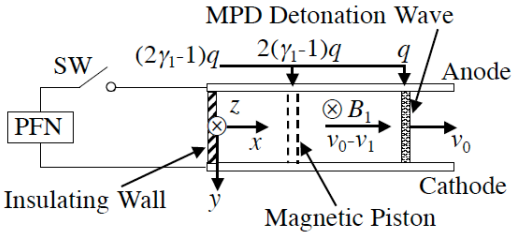

Figure 1. Pulsed MPD detonation thruster.

Prior to detonation analyses in the next section, contrasts and differences between the MPD detonation (MD) and the combustion detonation (CD) are summarized below.

1) Electrical input energy and propellant mass per shot are independent parameters of the MD propulsion, which make specific impulse variable. In the CD, on the other hand, the heat generated per unit mass is a chemical constant specific to propellant species.
2) Electrical energy is fed into the MD wave as Joule heating and mechanical work by Lorenz force via the electrodes and an arc discharge. The combustion heat in the CD is distributed in the reaction chamber in proportion to gas density.
3) Plasma flow behind the MD wave is sustained by the magnetic piston as sketched in Fig. 1. This feature lasts until the end of pulsed discharge. When the CD processes are completed, the burnt gas expands and stays stagnant in the combustion chamber as to satisfy boundary condition at the closed end.

The gas just in front of the MD wave at $x = x_{0+}$ in Fig. 2 is affected by the energetic electrons and radiation emitted from the arc discharge. The pressure P^* of ordinate consists o f magnetic and plasma pressures as will be defined later. As the avalanche discharge proceeds, the plasma is accelerated and compressed by Lorenz force as well as ionized and thermalized by Joule heating. Starting from the initial state "0", the typical CD wave is led by a shock wave and with a certain delay time, the chemical combustion is ignited as shown by adiabatic curves in Fig. 3 [2, 6]. Afterwards the burnt gas expands to the state "1", Chapman Jouguet (C-J) point in detonation adiabatic. It is

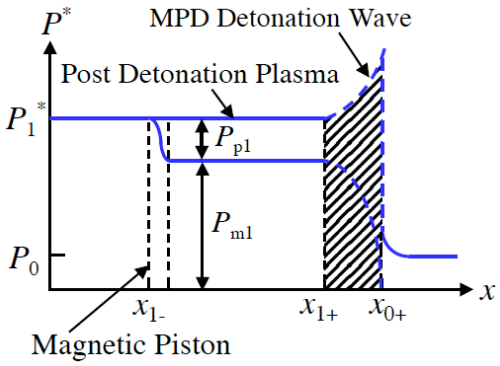

Figure 2. Generalized pressure P^* distribution along electrodes during pulse discharge at $t = t1 < \tau$ in Fig. 4.

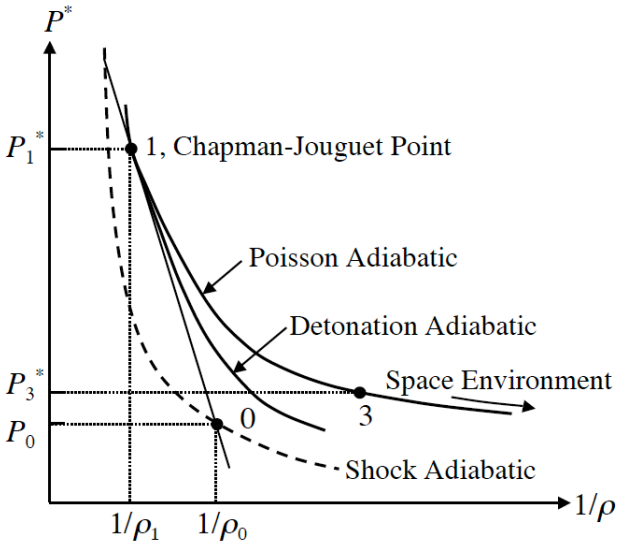

Figure 3. Adiabatic curves related to detonation and post-detonation processes.

uncertain whether a shock wave precedes in the MD wave. If the shock wave were to exist, it would be either an ion acoustic or a magnetosonic shock wave, although the latter seems unlikely within the MD wave. The magnetic expansion following the magnetosonic shock wave implies the discharge current to reverse from the cathode to anode. From the interest in jump conditions across the MD wave, expressing the uncertainty above by dashed lines in Fig. 2, we assume the C-J condition in the following analyses.

III. Magnetoplasmadynamic Detonation

The ordinates in Figs. 2 and 3 indicate magnetoplasmadynamic pressure P^*, which comprises plasma pressure P_p and magnetic pressure P_m as follows.

$$\begin{aligned} P^* &= P_m + P_p \,, \\ P_m &= B^2/2\mu \,, \\ P_p &= P_e + P_i \,, \end{aligned} \tag{1}$$

where B represents magnetic field intensity, and μ magnetic permeability. Suffixes in the order of m, p, e, and i represent the magnetic field, plasma, electron and ion. With ratio of specific heats γ, the thermodynamic relations among enthalpy h^*, internal energy e^*, density ρ and P^* are generalized and expressed by[4]

$$\begin{aligned} h^* &= e^* + P^*/\rho \\ &= \frac{\gamma}{\gamma - 1}\frac{P^*}{\rho} \\ &= \frac{\gamma_m}{\gamma_m - 1}\frac{P_m}{\rho} + \frac{\gamma_p}{\gamma_p - 1}\frac{P_p}{\rho} \quad . \end{aligned} \tag{2}$$

The enthalpy is also expressed as

$$h^* = \frac{c_m^2}{\gamma - 1}, \tag{3}$$

using magnetosonic velocity $c_m = \left(\gamma P^*/\rho\right)^{1/2}$.

Jump conditions across the one-dimensional MD wave are derived from conservation equations,

$$\rho_1 v_1 = \rho_0 v_0 = m \quad , \tag{4}$$

$$P_1^* + \rho_1 {v_1}^2 = P_0 + \rho_0 {v_0}^2 \quad , \tag{5}$$

$$\frac{{v_1}^2}{2} + h_1^* = \frac{{v_0}^2}{2} + h_0 + q \quad , \tag{6}$$

taking forward state "0" at $x = x_{0+}$ and aft state "1" at $x = x_{1-}$ in Fig. 2. Parameter q is the input energy to the MD wave. From Eqs. (4) and (5), mass flux m is derived as

$$m^2 = \left(P_1^* - P_0^*\right)/\left(1/\rho_0 - 1/\rho_1\right) \quad . \tag{7}$$

The Chapman – Jouguet condition mentioned earlier corresponds to the contact point of a tangent from "0" to "1" in Fig. 3, satisfying $dm^2/dP^* = 0$ and the minimum entropy in the MD adiabatic. At this point v_1 becomes magnetosonic velocity given by

$$\begin{aligned} v_1^2 &= c_{m_1}^2 \\ &= \gamma_1 P_1^* / \rho_1 \end{aligned} . \tag{8}$$

In the case of strong detonation $q >> e_0$ as assumed hereafter, Eqs. (4) – (6) are solved, giving

$$\begin{aligned} v_0^2 &= 2\left(\gamma_1{}^2 - 1\right)q, \\ v_0 - v_1 &= v_0/\left(\gamma_1 + 1\right), \\ \rho_0/\rho_1 &= \gamma_1/\left(\gamma_1 + 1\right). \end{aligned} \tag{9}$$

These results are obtained with reference to the frame moving with the MD wave. In order to apply the results to propulsion performance Eq. (6) is rewritten in the thruster frame, i.e. the stationary gas in "0" state.

$$m\left\{\frac{\left(v_0 - v_1\right)^2}{2} + e_1^*\right\} = m\left(e_0 + q\right) + P_1^*\left(v_0 - v_1\right) \tag{10}$$

The left hand side of above equation represents the kinetic and internal energy of magnetized plasma behind the MD wave. In the right hand side are "0" state internal energy, the input energy and work done by the magnetic piston which moves at $v_0 - v_1$ supporting the backside of uniform plasma flow behind the MD wave as shown in Fig. 1 and the *x-t* diagram Fig. 4. The discharge current is concealed within the MD layer of the order of $1/\sigma\mu V$ in thickness estimated with representative electrical conductivity σ and velocity V (Ref. 7). The post MD plasma between the magnetic piston at $x = x_{1-}$ and the MD wave at $x = x_{0+}$ can move inertially under the back electromotive force $(v_0 - v_1)B_1$ which cancels transverse electric field. The distribution of P^* along the horizontal line $t = t_1$ in Fig. 4 has been given in Fig. 2, where the P_m jump across the magnetic piston at $x = x_{1-}$ is qualitatively drawn as balancing the pressure P_{p1} behind the MD wave. In the following of this section are analyzed two cases: the one with electromagnetic energy dominating over ionization energy and the other with these two effects comparable.

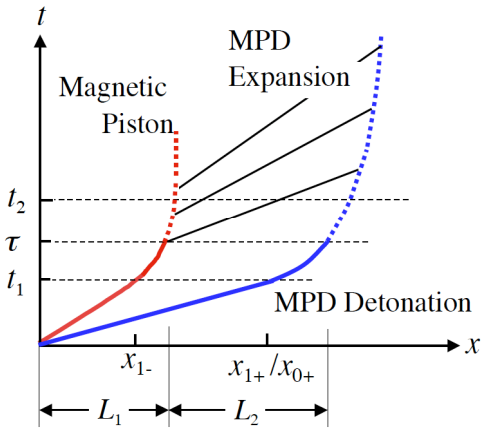

Figure 4. Space-time diagram of detonation wave propagation.

A. Fully ionized plasma dominated by electromagnetic effects.

In addition to the strong detonation and C-J conditions, the post MD plasma is assumed fully ionized and to have total energy far exceeding ionization energy. The energy composition related to propulsive performance is found further rewriting Eq. (10).

$$\frac{\left(v_0 - v_1\right)^2}{2} + h_1^* = h_0 + q + \frac{\left(P_1^* - P_0\right)}{\rho_0} \tag{11}$$

The terms in the left hand side of this equation are calculated using Eq. (9).
Kinetic energy:

$$\left.\begin{aligned} &\frac{(v_0 - v_1)^2}{2} = \frac{\gamma_1 - 1}{\gamma_1 + 1} q \qquad (11\,\%) \\ &\text{Enthalpy:} \\ &h_1^* = \frac{v_1^2}{\gamma_1 - 1} \qquad (89\,\%) \end{aligned}\right\} \tag{12}$$

The fractional figures in the parenthesis are estimated by taking $\gamma_1 = 2$ for the post MD adiabatic plasma. The large fractional value of enthalpy implies the importance of plasma expansion process after the completion of the pulsed discharge. It is noteworthy that the total energy in Eq. (11) amounts to $(2\gamma_1 - 1)q$, which comprises the input energy to the detonation wave q and the work done by the magnetic piston $2(\gamma_1 - 1)q$. The total energy is delivered from a single energy source and self-consistently split into two current paths as sketched in Fig. 1.

B. Critical velocity ionization phenomena

The condition that the plasma becomes fully ionized was experimentally observed in an MPD arcjet experiment[8] and explained in the light of Alfvén's critical velocity condition[9] which asserts the equi-partition of plasma kinetic and ionization energy. There are two ways in applying the condition: one in the frame of MD wave, and the other in the thruster frame.

1. Detonation frame

The energy balance in this case is expressed by adding a term eV_i/m_i to each side of Eq. (6) and denoting the post MD condition as state "2", where v_i is the ionization potential and m_i is the ion mass.

$$\frac{v_2^2}{2} + h_2^* + \frac{eV_i}{m_i} = \frac{v_0^2}{2} + h_0 + q + \frac{eV_i}{m_i} \tag{13}$$

One can consider $Q = q + eV_i/m_i$ renewed input energy to the MD wave. The Alfvén's condition requires that the first and third terms be equal in the left hand side of Eq. (13), namely the critical velocity $v_{cr} = (2eV_i/m_i)^{1/2}$ is given by

$$v_{cr} = v_2 = c_{m2} \ , \tag{14}$$

which with reference to Eqs. (3) and (8) is found equivalent to the C-J condition. The close relationship between v_{cr} and c_m has been experimentally and analytically confirmed[10]. In a similar manner to the preceding section the energy contents in the post MD plasma are calculated.

$$\left.\begin{aligned} &\text{Kinetic energy:} \\ &\frac{v_2^2}{2} \qquad (22\%) \\ &\text{Enthalpy:} \\ &h_2^* = \frac{v_2^2}{\gamma_2 - 1} \qquad (56\%) \\ &\text{Ionization energy:} \end{aligned}\right\} \tag{15}$$

$$\frac{eV}{m_i} = \frac{v_2^2}{2}, \quad (22\%)$$

where $\gamma_2 = 1.8$ is used assuming the magnetic and plasma terms equal in Eq. (2) for $\gamma_m = 2$ and $\gamma_p = 5/3$. The ionization energy is abandoned as frozen flow loss when the plasma expands into space.

2. Thruster frame

The critical velocity with reference to the thruster frame is given by $v_{cr} = v_o - v_2$. In the same way as the preceding section, eV_i/m_i is added to the both sides of Eq. (11)

$$\begin{aligned} &\frac{\left(v_0 - v_2\right)^2}{2} + h_2^* + \frac{eV_i}{m_i} \\ &= h_0 + q + \frac{eV_i}{m_i} + \frac{\left(P_2^* - P_0\right)}{\rho_0} \\ &= h_0 + Q + \frac{\left(P_2^* - P_0\right)}{\rho_0}. \end{aligned} \tag{16}$$

The energy contents in the post MD plasma are calculated for $\gamma_2 = 1.8$.

Kinetic energy:

$$\frac{\left(v_0 - v_2\right)^2}{2} \quad (10\%)$$

Enthalpy:

$$h_2^* = \frac{\gamma_2^2\left(v_1 - v_2\right)^2}{\gamma_2 - 1} \quad (80\%)$$

Ionization energy:

$$\frac{eV_i}{m_i} = \frac{\left(v_0 - v_1^2\right)^2}{2} \quad (10\%) \tag{17}$$

IV. Magnetoplasmadynamic Expansion and Thruster Design

When the pulsed discharge ends at $t = \tau$, the magnetic piston and the MD wave are gradually weakened spending residual energy in the circuit as sketched by dashed lines in Fig. 4. Afterwards the post MD plasma is caught up by an expansion front moving at magnetosonic speed and further swept by expansion fan. The pressure distribution along the line $t = t_2$ ($> \tau$) in Fig. 4 is illustrated in Fig. 5. The equation governing inter-electrode magnetic and flow fields is generally described by Maxwell's equation and Ohm's law.

$$\frac{\partial B}{\partial t} + \frac{\partial}{\partial x}\left(Bv\right) - \frac{1}{\sigma\mu}\cdot\frac{\partial^2 B}{\partial x^2} = 0. \tag{18}$$

When the variables are normalized by the representative values of electrical conductivity σ, flow velocity V and length L, the coefficient of last term is found inversely proportional to the magnetic Reynolds number $R_m = \sigma\mu VL$ (Ref. 6). For large R_m Eq. (18) is reduced to

$$\frac{\partial B}{\partial t} + \frac{\partial}{\partial x}(Bv) = 0 \quad . \tag{19}$$

When B is replaced by ρ, this equation resembles to the mass conservation equation

$$\frac{\partial \rho}{\partial t} + \frac{\partial}{\partial x}(\rho v) = 0 \quad . \tag{20}$$

The comparison of these equations suggests that the magnetic field B is proportional to the density ρ, giving adiabatic relations $P_m \propto \rho^2$ and $\gamma_m = 2$ for Eq. (1). If these descriptions are valid in the region $x_{1-} < x < x_1$ in Fig. 5, the processes therein are considered adiabatic MPD expansion. The expansion of magnetic field in the post MD plasma accompanies a reverse current, which, driven by the back electromotive force established behind the MD wave, flows from the cathode to anode.

From the foregoing analyses and discussions it is suggested as a design guideline to take full advantage of the high enthalpy plasma in section L_2 in Fig. 4. The plasma, if freely expands backward after the discharge pulse, tends to fill the void, section L_1 in Fig. 4 with plasma pressure as high as P_3^* (Ref. 6)

$$P_3^* = P_1^* \left\{ 1 - \frac{1}{2}(\gamma_1 - 1)\frac{v_0 - v_1}{c_{m1}} \right\}^{2\gamma_1/(\gamma_1 - 1)} \tag{21}$$

The thrust loss due to the backward expansion can be minimized by designing the L_1 section as a narrow parallel channel, while thrust generation can be maximized by designing L_2 section as a diverging nozzle and thereby fully expanding the plasma into space environment of much lower pressure than P_3^*. To summarize the thruster electrodes are suggested to have

1) a narrow parallel section of length $L_1 = \tau(v_o - v_1)$ in the upstream , followed by
2) a diverging section of length $L_2 = \tau\, v_1$ in the downstream

for the velocities v_0 and v_1 given by Eq. (9) and pulse width τ.

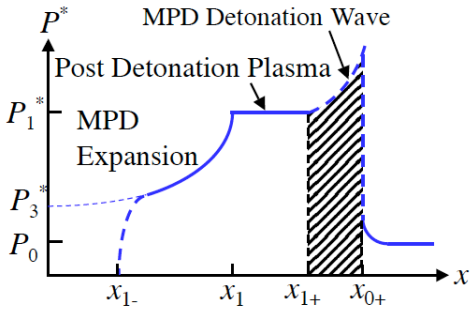

Figure 5. Generalized pressure *P distribution along electrodes after pulse discharge at $t = t2 > \tau$ in Fig. 4.**

V. Related Former Studies

In an experiment of PPT the current reversal was revealed by magnetic probe measurement[11]. The results of equi-intensity lines of magnetic field or stream lines of current near zero discharge current are reproduced in Fig. 6. The current reversal in the MPD expansion explained above is found in the left side of Fig. 6, and together with the onward current in the MD front constitutes a vortex. Also in the middle of Fig. 6 is found the area of diffuse current, which corresponds to the plateaus of P^* in Figs. 2 and 5.

The thrust performance of a PPT was experimentally obtained for comparing straight and flared electrodes[12]. As

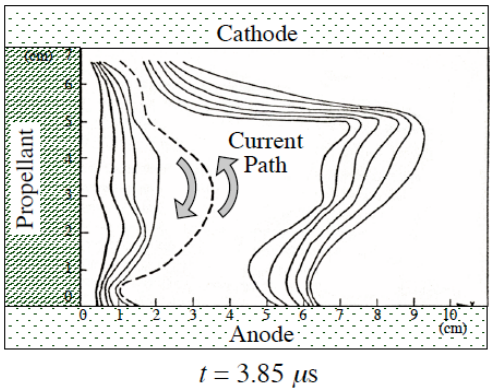

Figure 6. Current vortex observed in a PPT. Current arrows are supplemented to the original reproduced from Ref. 11.

shown in Fig. 7, the flared configuration demonstrated about 30 % increase in impulse bit comparing with planar configuration. Even electrically insulating nozzle, though used in a quasi-steady MPD arcjet, was found to enhance the generation of electromagnetic thrust[13]. The swirling current similar to the one in Fig. 6 is considered effective in trapping magnetized plasma inside and exerting electromagnetic thrust to the diverging wall.

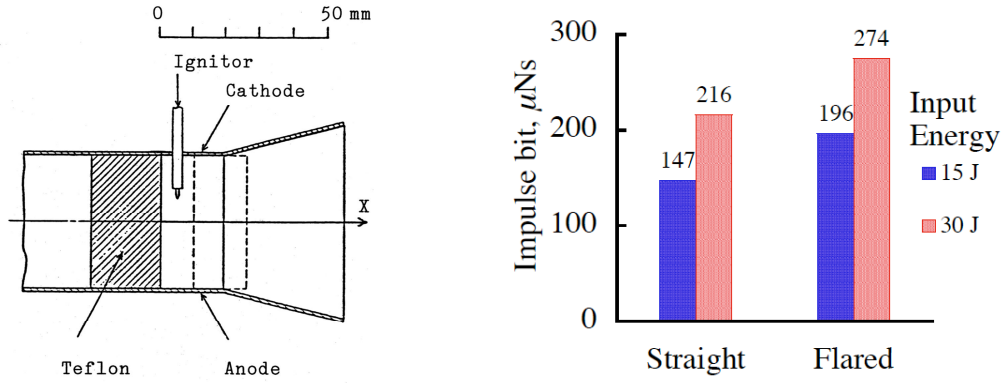

(a) Cross sectional view of flared

(b) Impulse bit of straight and flared PPT's.

Figure 7. Thrust enhancement of PPT resulted from flared electrode configuration.[12] Self-field operation.

VI. Conclusions

With respect to the pulsed magnetoplasmadynamic (MPD) detonation propulsion, following results were obtained.

1) The one-dimensional detonation driven by a magnetic piston was formulated with generalized MPD thermodynamic relations, and jump conditions corresponding to Chapman-Jouguet point were obtained for given electrical input energy.
2) The energy composition in post MPD detonation wave was obtained to evaluate the thrust performance with reference to thruster frame. From the large fraction found in the enthalpy of post detonation plasma a design guideline to enhance thrust production was suggested.
3) Ionization effects were taken into account referring to the Alfvén's critical velocity condition, which was found closely related to the Chapman-Jouguet detonation condition.

References

[1] Benson, S. W. and Hosleins, W. A., "Development of a PPT for the EO-1 Spacecraft," 35th Joint Propulsion Conference and Exhibit, AIAA-99-2276, Los Angels, USA, 1999.

[2] Jahn, R. G., "Physics of Electric Propulsion," McGraw Hill Book Co., 1968.

[3] Landau, L. D. and Lifshitz, E. M. "Fluid Mechanics," Pergamon Press, 1959.

[4] Kuriki, K. and Nakayama, T. "Magnetosonic Condition in Magnetoplasmadynamic Flow," *Journal of Propulsion and Power*, Vol. 8, No. 6, 1992, pp. 1208-1211.

[5] Markusic, T. E. and Choueiri, E. Y. "Visualization of Current Sheet Canting in a Pulsed Plasma Accelerator," 26th International Electric Propulsion Conference, IEPC-99-206, Kitakyushu, Japan, 1999.

[6] Bussing, T. and Pappas, G. "Pulse Detonation Engine Theory and Concepts," Progress in Astronautics and Aeronautics, AIAA, Reston, VA, ed. Murthy, S. N. B. and Curran, E, T. Vol. 165, 1996. pp. 421-472.

[7] Kuriki, K., Kunii, Y. and Shimizu, Y. "Current distribution in Plasma Thruster," AIAA/JSASS/DGLR 15th International Electric Propulsion Conference, AIAA-81-0685, 1981.

[8] Kuriki, K. and Suzuki, H. "Transitional Behavior of MPD Arcjet Operation," *AIAA Journal*, Vol. 16, No. 10, 1978, pp. 1062-1067.

[9] Alfvén, H. "Collision between a Non-Ionized Gas and a Magnetized Plasma," *Reviews of Modern Physics*, Vol. 32, 1960, pp. 710-713.
[10] Brenning, N. "Reviews of the CIV Phenomenon," *Space Science Reviews*, Vol. 59, 1992, pp. 209-314.
[11] Palumbo, D. J. and Begun, M. "Plasma Acceleration in Pulsed Ablative Arc Discharges," AFOSR TR-77-0623, 1977.
[12] Takegahara, H. "Effect of Applied Magnetic Fields on a Solid Propellant Pulsed Plasma Thruster," Dr. Eng. Dissertation, Dept. Aerospace Engineering, University of Tokyo, Tokyo, Japan, 1985. (in Japanese)
[13] Nishida, E., Shimizu, Y. and Kuriki, K. "Improved Thrust Generation Mechanism for Electrothermal/Electromagnetic Arcjet," 20th International Electric Propulsion Conference, IEPC-88-026, Garmisch-Partenkirchen, West Germany, 1988.